

Electronic Supplementary Information

Mechanistic studies on lithium intercalation in a lithium-excess layered material using

Li_2RuO_3 epitaxial film electrodes and *in situ* surface X-ray analysis

Sou Taminato,^a Masaaki Hirayama,^{*a} Kota Suzuki,^a KyungSu Kim,^a Kazuhisa Tamura,^b

Jun'ichiro Mizuki^b and Ryoji Kanno^a

^a Department of Electronic Chemistry, Tokyo Institute of Technology, 4259 Nagatsuta-cho,

Midoriku-ku, Yokohama 226-8502, Japan

^b Japan Atomic Energy Agency, Synchrotron Radiation Research Center, Kansai Research

Establishment, 1-1-1 Kouto, Sayo-cho, Sayo-gun, Hyogo 679-5148, Japan

*Phone: +81459245503

*E-mail: hirayama@echem.titech.ac.jp

X-ray reflectivity analysis

Figure S1 presents typical X-ray reflectivity (XRR) spectra of the (010) and (001) films, acquired in air using a thin-film X-ray diffractometer (ATX-G, $\text{CuK}\alpha_1$). The spectra are plotted as a function of the scattering vector, $Q_z = 4\pi(\sin\theta)/\lambda$, where λ is the wavelength of the X-rays (1.541 Å) and θ is the incident angle. The thickness of each film was estimated by applying the Fourier transform technique to these X-ray reflectivity curves. The thickness, density and roughness of the films were refined using the Parratt32 data analysis program, with reflectivity values calculated using Parratt's method.¹ A four-layer model composed of the SrTiO_3 substrate, an interfacial layer between the SrTiO_3 and the Li_2RuO_3 , the Li_2RuO_3 film and a surface layer provided the best fits to the reflectivity curves and the fitting parameters are summarized in Table S1. The surface layer was found to have a density of approximately 2 g cm^{-3} , significantly lower than that of the Li_2RuO_3 layer (ca. 5.1 g cm^{-3}). Low density surface impurity phases such as Li_2CO_3 ($\rho = 2.1 \text{ g cm}^{-3}$) and LiOH ($\rho = 1.5 \text{ g cm}^{-3}$) are often formed on lithium intercalation materials due to surface reactions with the moisture and carbon dioxide in the surrounding air.²⁻⁵ The low density of the surface layer therefore suggests the formation of one or more of these impurity phases on the bare Li_2RuO_3 electrode. No significant differences in density and roughness were observed between the (010) and (001)

films. In addition, the results of analyses of films with different thicknesses indicated that there was no significant correlation between the film thickness and the density or roughness.

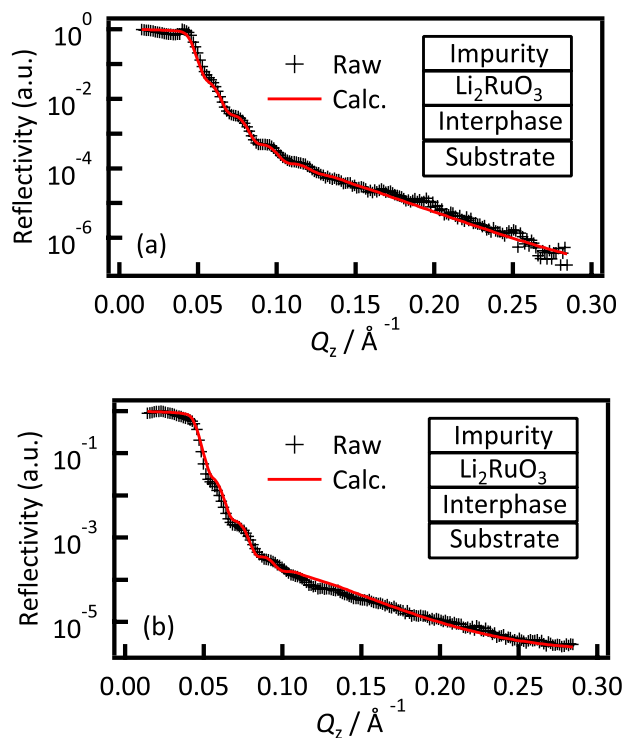


Figure S1. XRR spectra and simulated curves for (a) (010) and (b) (001) films. The insets show simulation models.

Table S1. XRR analysis results for (010) and (001) films.

	Thickness, t (nm)	Density, d (g cm ⁻³)	Roughness, r (nm)
(a) Li ₂ RuO ₃ (010) film			
Surface layer	2.3	2.02	0.6
Li ₂ RuO ₃	23.7	5.19	2.0
Interphase	4.3	4.79	1.8
SrTiO ₃ substrate	-	5.12	2.2
(b) Li ₂ RuO ₃ (001) film			
Surface layer	3.0	1.92	0.6
Li ₂ RuO ₃	24.3	5.10	2.1
Interphase	5.2	4.79	2.1
SrTiO ₃ substrate	-	5.12	2.2

Thickness dependence of cell parameters

Figure S2 shows the variations in the d values of the 004 and 060 peaks of the (010) and (001) films with film thickness. The values of the 004 and 060 peaks are distributed within the ranges of 2.38–2.44 Å and 1.46–1.48 Å, respectively. These results also support our finding that there is no significant effect of film thickness on the Li_2RuO_3 thin films. Hence, the (010) and (001) films provide a two-dimensional reaction field suitable for modeling the lattice plane dependence of electrode reactions.

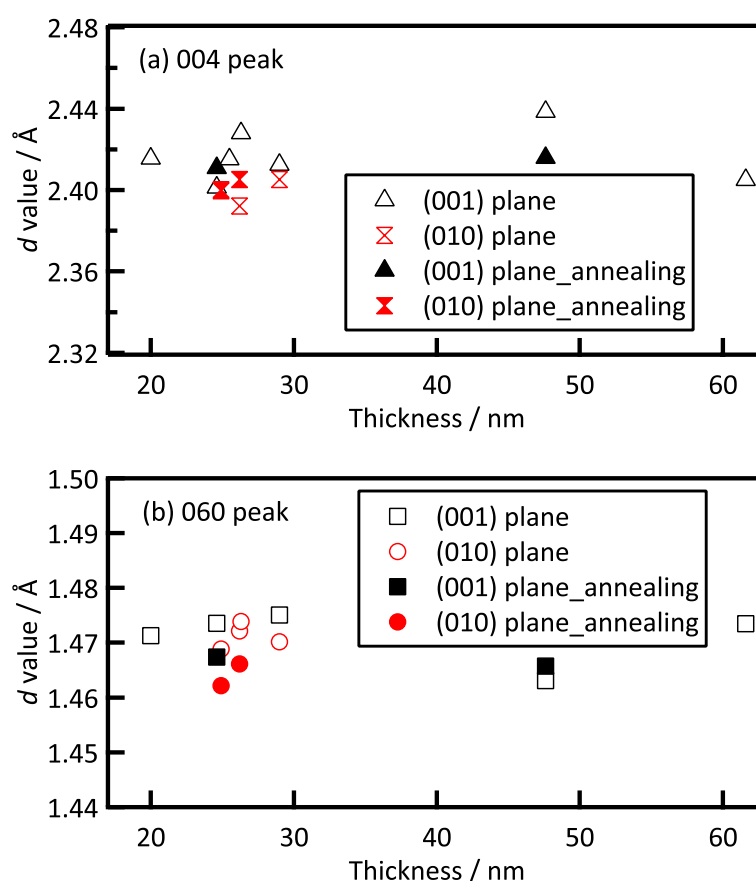


Figure S2. Thickness dependence of d values of (a) 004 and (b) 060 peaks of Li_2RuO_3 thin films. Filled symbols in each figure indicate data obtained for films after annealing.

Bulk structure change of the (010) film along in-plane direction

Figure S3 shows the XRD pattern of the in-plane 202 diffraction peak for a 61.6 nm-thick $\text{Li}_2\text{RuO}_3(010)$ film after electrochemical cycling. The charge/discharge test was performed using a coin-type cell, and then the cell was disassembled. The film was washed in ethanol solution, and the in-plane XRD pattern was collected in air using an incident angle of 0.36° which is higher than the critical angle of Li_2RuO_3 . The penetration depth of X-ray ($\text{Cu-K}\alpha$) was calculated to be 57 nm at the incident angle, which indicates that the in-plane XRD pattern corresponds to the structural change throughout the film. No additional diffraction peak was observed except for the 202 peak of Li_2RuO_3 . This result confirms that no irreversible phase transition occurred along the in-plane direction at the $\text{Li}_2\text{RuO}_3(010)$ bulk during the electrochemical reactions. This supports that the irreversible phase change of the (010) film detected by the *in situ* in-plane XRD measurements occurred at the surface region (Figs. 5 and 6), because the XRD patterns were collected using low incident angles of X-rays below the critical angle of Li_2RuO_3 .

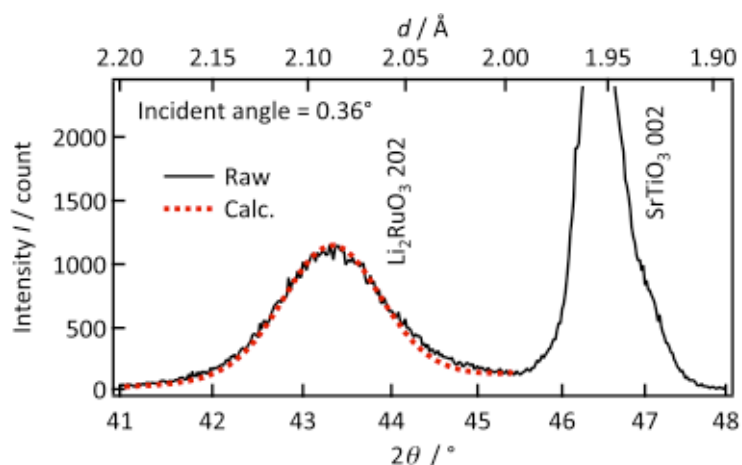


Figure S3 XRD pattern of the in-plane 202 diffraction peak for a 61.6 nm-thick $\text{Li}_2\text{RuO}_3(010)$ film after electrochemical cycling.

Lithium diffusion pathways in Li_2RuO_3

Figure S4 shows the possible diffusion pathways of lithium in the ab plane and along the c axis in Li_2RuO_3 with the $C2/c$ space group. The (010) film has two-dimensional $[\text{LiO}_6]$ and $[(\text{Li,Ru})\text{O}_6]$ layers perpendicular to the electrolyte, which has an interlayer Li diffusion pathway between the octahedral $4e$ sites through the interstitial tetragonal $8f$ site in the ab plane. In contrast, the (001) film, in which these layers are parallel to the electrolyte, has the Li diffusion pathway through the $[\text{LiO}_6]$ and $[(\text{Li,Ru})\text{O}_6]$ slabs along the c axis. The lithium ions diffuse from the octahedral $4e$ sites in the $[\text{LiO}_6]$ layer to the octahedral $4d$ sites in the $[(\text{Li,Ru})\text{O}_6]$ layer through the interstitial tetragonal $8f$ site. The interstitial LiO_4 tetrahedra and the LiO_6 octahedra share their faces in the ab plane and along the c direction. The sizes of the

bottlenecks associated with lithium diffusion in the ab plane and along the c axis are 4.03 \AA^2 and 3.68 \AA^2 , respectively, based on calculations using the crystal structure of polycrystalline Li_2RuO_3 .⁶ The larger opening available for lithium diffusion along the ab plane as compared to along the c axis therefore leads us to expect faster lithium diffusion in the ab plane. The anisotropic activation energies of lithium diffusion in the lithium-excess layered material Li_2MnO_3 , with a similar crystal structure to Li_2RuO_3 , have been determined by first-principles calculations. The results of these calculations confirm the bottleneck evidence, since the calculated activation energy of lithium diffusion along the ab plane (0.61 eV) is lower than that along the c axis (0.73 eV).⁷

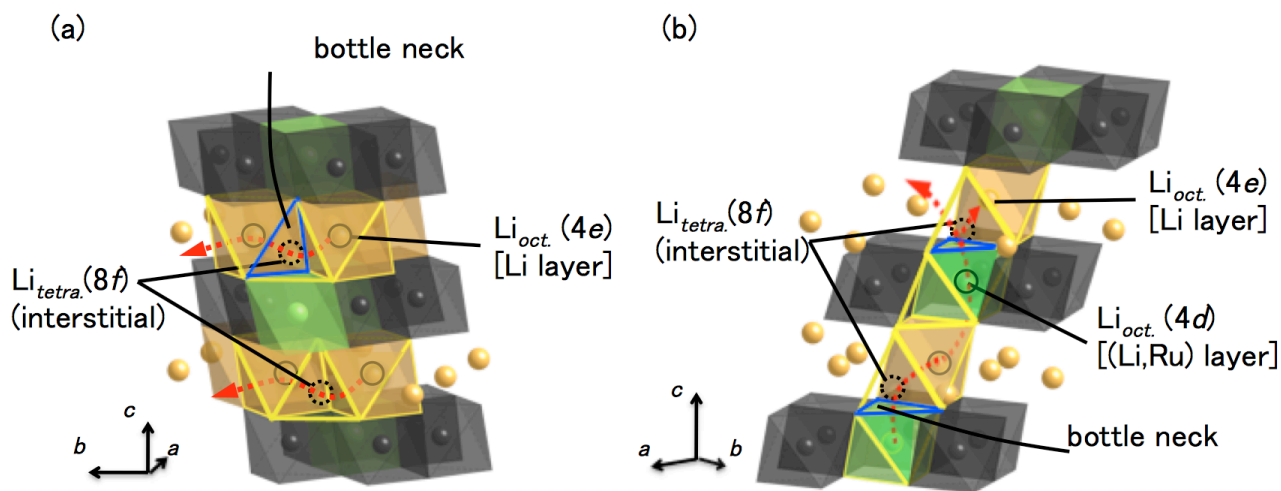


Figure S4. Possible lithium diffusion pathways in Li_2RuO_3 along the (a) (010) and (b) (001) directions.

References

- 1 L. G. Parratt, *Physical Review*, 1954, **95**, 359-369.
- 2 M. Hirayama, N. Sonoyama, M. Ito, M. Minoura, D. Mori, A. Yamada, K. Tamura, J. Mizuki and R. Kanno, *Journal of the Electrochemical Society*, 2007, **154**, A1065-A1072.
- 3 M. Hirayama, N. Sonoyama, T. Abe, M. Minoura, M. Ito, D. Mori, A. Yamada, R. Kanno, T. Terashima, M. Takano, K. Tamura and J. Mizuki, *Journal of Power Sources*, 2007, **168**, 493-500.
- 4 M. Hirayama, K. Sakamoto, T. Hiraide, D. Mori, A. Yamada, R. Kanno, N. Sonoyama, K. Tamura and J. Mizuki, *Electrochimica Acta*, 2007, **53**, 871-881.
- 5 M. Hirayama, M. Yonemura, K. Suzuki, N. Torikai, H. Smith, E. Watkins and J. Majewski and R. Kanno, *Electrochemistry*, 2010, **78**, 413-415.
- 6 H. Kobayashi, R. Kanno, Y. Kawamoto, M. Tabuchi, O. Nakamura and M. Takano, *Solid State Ionics*, 1995, **82**, 25-31.
- 7 R. Xiao, H. Li and L. Chen, *Chemistry of Materials*, 2012, **24**, 4242-4251.